

Numerical simulation of density-driven natural convection in porous media with application for CO₂ injection projects

Rouhollah Farajzadeh*, Hamidreza Salimi, Pacelli L.J. Zitha, Hans Bruining

Delft University of Technology, Department of Geotechnolgy, Stevinweg 1, 2628 CN Delft, The Netherlands

Received 23 February 2007; received in revised form 17 August 2007

Available online 23 October 2007

Abstract

In this paper we investigate the mass transfer of CO₂ injected into a homogenous (sub)-surface porous formation saturated with a liquid. In almost all cases of practical interest CO₂ is present on top of the liquid. Therefore, we perform our analysis to a porous medium that is impermeable from sides and that is exposed to CO₂ at the top. For this configuration density-driven natural convection enhances the mass transfer rate of CO₂ into the initially stagnant liquid. The analysis is done numerically using mass and momentum conservation laws and diffusion of CO₂ into the liquid. The effects of aspect ratio and the Rayleigh number, which is dependent on the characteristics of the porous medium and fluid properties, are studied. This configuration leads to an unstable flow process. Numerical computations do not show natural convection effects for homogeneous initial conditions. Therefore a sinusoidal perturbation is added for the initial top boundary condition. It is found that the mass transfer increases and concentration front moves faster with increasing Rayleigh number. The results of this paper have implications in enhanced oil recovery and CO₂ sequestration in aquifers.
© 2007 Elsevier Ltd. All rights reserved.

Keywords: Natural convection; CO₂; Porous media; Density driven; Mass transfer

1. Introduction

The growing concerns over the global heating due to the increase in the global concentration of greenhouse gases in the atmosphere have increased the interest in examining various techniques to reduce the emission of these gases, in particular CO₂, into the atmosphere. One viable technique is to inject CO₂ into geological formations, for example, oil and gas reservoirs, deep saline aquifers and coal beds. In many practical cases, geological storage of CO₂ is accomplished by injecting it in dense form into a porous rock formation below the earth's surface which is already saturated with a liquid (water or oil). Therefore, quantification of CO₂ dissolution in (sub)-surface fluids is of paramount importance in CO₂ sequestration projects.

The densities of the water–CO₂ and oil–CO₂ solutions increase with increasing CO₂ concentration [1,2]. Hence it

is expected that when CO₂ is injected into the porous formation, initially the injected CO₂ accumulates under the cap rock and subsequently dissolves into the formation liquid by molecular diffusion [3]. As a result, the density of liquid increases and eventually CO₂–liquid interface becomes unstable. For favorable conditions, natural convection occurs and enhances the mass transfer of CO₂. Significant enhancement in the mass transfer rate of CO₂ into water [4,5] and oil (*n*-decane) [5] at elevated pressures has been reported in only a few published experimental investigations on this subject. In [5] it has been asserted that in the initial stages of the process, natural convection and diffusion are the processes governing the mass transfer of CO₂ into water and oil. Nevertheless, after a certain time, depending on the geometry of the system and the initial pressure, diffusion will be the dominant mechanism. Hence, the mass transfer of CO₂ into water and oil cannot be modeled with Fick's law with a single diffusion coefficient due to natural convection effects. However, the convection effects die out with time.

* Corresponding author. Tel.: +31 015 278 7961; fax: +31 015 278 1189.
E-mail address: r.farajzadeh@tudelft.nl (R. Farajzadeh).

Nomenclature

A	aspect ratio, H/L [-]	<i>Greek symbols</i>	
c	dimensionless concentration [-]	α	wave-number
c'	concentration [mol/m^3]	β_c	volumetric expansion factor [m^3/mol]
D	diffusion coefficient [m^2/s]	δ	amplitude [-]
g	acceleration due to gravity [m/s^2]	ϕ	porosity of the porous medium [-]
Gr	Grasshof number [-]	λ	wavelength [-]
H	height of the porous medium [m]	μ	viscosity of the fluid [$\text{kg}/\text{m s}$]
k	permeability of the porous medium [m^{-2}]	ψ	stream function [$\text{m}^3 \text{m}^{-1} \text{s}^{-1}$]
k_H	Henry's solubility constant [$\text{Pa}/\text{mol}/\text{m}^3$]	ρ	density of the fluid [kg/m^3]
L	length of the porous medium [m]	σ	dimensionless growth rate [-]
P	pressure [Pa]	τ	dimensionless time [-]
Ra	Rayleigh number [-]	<i>Subscripts</i>	
t	time [s]	0	value of the quantity at the boundary
u	dimensionless velocity [-]	i	reference value of the quantity
U	velocity [m/s]	x	quantity in x -direction
z	distance from the bottom of the tube [m]	z	quantity in z -direction
x	dimensionless distance in X -coordinate		
z	dimensionless distance in Z -coordinate		

Several authors have studied the problem of occurrence of natural convection in a saturated porous layer subject to a sudden temperature rise from the bottom. Foster [6] showed that the critical time that elapses before the onset of the instability is independent of the depth of fluid layer for large Rayleigh numbers, a result which was verified experimentally [7]. Lapwood [8] determined the criterion for the onset of natural convection, which occurs at Rayleigh numbers above $4\pi^2 \approx 40$. Elder [9] and Wooding [10] suggested imposing small perturbations to the initial condition to observe the fingers of hot fluid protruding into the porous medium. Foster [6] stated that the fluid manifests convective behavior or “onset of instability” when the averaged vertical velocity disturbance had increased by a factor between one and three orders of magnitude of its initial value. Results of Foster [6] and Lapwood [8] showed that the critical time required for the onset of natural convection is inversely proportional to the square of permeability of the porous medium. Indeed the interface of two immiscible fluids can be unstable due to several mechanisms in the porous medium. The stability of saturated porous layer under natural convection effects by means of a linear stability analysis, the energy method and a two dimensional numerical model have been studied by several researchers and the criteria in which the boundary becomes unstable have been reported in the literature [11–15]. The results of these investigations show that the critical (fastest growing) wavelength for the onset of natural convection is inversely proportional to the Rayleigh number or the permeability of the porous medium. This means that for the high permeable reservoirs the conventional simulators will not give satisfactory results, since a very high resolution is required to numerically simulate such a problem.

The analogy between heat and mass transfer phenomena allows us to use the same equations for natural convection driven by temperature variations as for natural convection driven by concentration variations. We have applied this analogy to study the effects of natural convection in a porous medium saturated with liquid (water or oil) when overpressurized CO_2 rich gaseous phase is in contact with the top. We investigate the effect of natural convection on the flow regime and quantify it numerically. The theory and the results described in this paper can be applied to CO_2 sequestration in aquifers and CO_2 flooding for oil recovery in porous media. Before we turn to the theory we describe one experimental result in detail. In this stage it is not possible to use the theory for the interpretation of the experiments, because (1) the theory is in Cartesian system coordinates, whereas the experiments are in cylindrical coordinates, which poses some difficult numerical problems and (2) the comparison would entail only a few experiments which can possibly lead to premature conclusions. Therefore, we leave the comparison between theory and experiments for future work.

2. Experimental

The schematic of the setup is shown in Fig. 1. It consists of a glass cell with the diameter of 7 mm and length of 45 cm. The cell is sealed and kept at constant temperature (for details see [5]). The glass tube was filled with sand grains (with an average diameter of 1 mm) up to the desired height ($L = 20$ cm) and then saturated with water. The small diameter of the glass tube allowed high pressure (11.6 bar) experiments, but possibly introduces boundary effects as much less than 50 grains (some 10 grains) are in a horizontal cross-section. The porosity of the sand pack

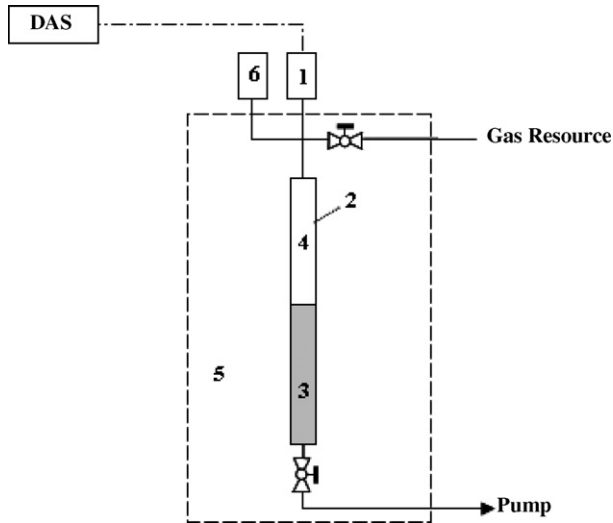


Fig. 1. Schematic of the experimental setup: (1) pressure transducer, (2) cell, (3) liquid phase, (4) gas phase, (5) the liquid bath, (6) pressure safety valve, (7) data acquisition system connected to a computer.

was measured as $\varphi = 0.42$. Using the Karman–Kozeny correlation the permeability was calculated to be $k = 1200$ Darcy. CO_2 was slowly injected into the cell from the top, for about 30 s. When the CO_2 pressure reached the desired value, the valve connecting to the gas source was closed and the cell was isolated. This was the starting time of the experiment. The gas pressure was recorded every 10 s in a computer.

Fig. 2 shows the experimental data (solid line) and the predicted pressure decline (dotted line) as calculated by Fick's law for stagnant water for an initial pressure $P_0 = 11.6$ bar. The dotted line was plotted by inserting a diffusion coefficient of $D = 2.0 \times 10^{-9} \text{ m}^2/\text{s}$ and Henry's solubility constant $k_H = 2980.1 \text{ Pa/mol/m}^3$ in the 1D diffusion model described in detail in Ref. [5].

It can be seen from Fig. 2 that the mass transfer of CO_2 in a porous medium saturated with water at slightly ele-

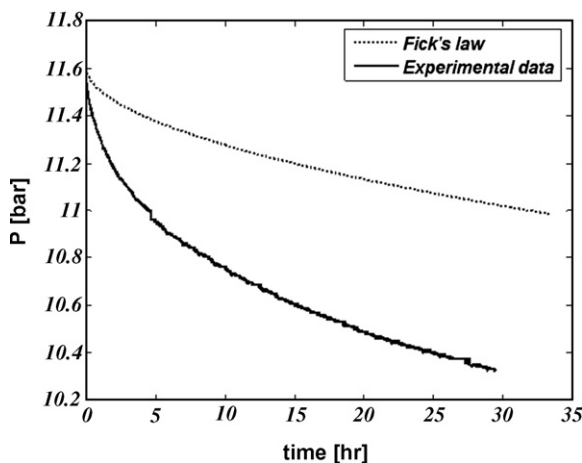


Fig. 2. Enhanced mass transfer of CO_2 into a porous medium saturated with water; the experimental pressure decline for the porous medium is faster than the diffusion model prediction.

vated pressure is significantly higher than the mass transfer expected in stagnant water in a porous medium, calculated by Fick's law at the same pressure, but much slower than the mass transfer in the absence of a porous medium. As mentioned in the introduction we assert that density-driven natural convection is the responsible mechanism for enhanced mass transfer of CO_2 into the water present in porous media.

3. Physical model

3.1. Formulation

If the fluid in the porous medium is in mechanical equilibrium in a gravitational field the concentration in the z -direction will be merely a function of the distance from the interface, i.e., $c = c(z)$. Nevertheless, if the concentration varies in the x -direction or if the vertical concentration gradient value exceeds a certain value, mechanical equilibrium is not possible and the fluid inside the porous medium starts to move to return the system to equilibrium. We try to formulate the occurrence of such phenomena.

Under consideration is the natural convection flow in a porous medium saturated with a fluid with a height H and length L . The permeability of the porous medium is k and its porosity is φ . The porous medium is impermeable on the left and right side. Initially the fluid is at rest and there is no CO_2 dissolved in the fluid. CO_2 is continuously supplied from the top, i.e., CO_2 concentration at the top is kept constant. We assume that CO_2 –liquid interface is relatively sharp and fixed. Moreover, we assume a no-flow boundary at the bottom of the porous medium. We disregard the presence of a capillary transition zone between the gas and the liquid phase. Hence we only model the liquid phase and the presence of the gas phase at the top is represented by a boundary condition for the liquid phase. The motion of fluid is described by Darcy's law driven by a density gradient. Darcy's law is combined with the mass conservation laws for the two components (CO_2 and either water or oil) to describe the diffusion and natural convection processes in the porous medium. We only expect a laminar regime since Rayleigh's number is low. The density gradient is the source of natural convection and therefore the density cannot be considered constant. However, we use Boussinesq approximation which considers density variations only when they contribute directly to the fluid motion.

3.2. Governing equations

For the 2D porous medium depicted in Fig. 3, the governing equations can be written as

(a) Continuity equation

$$\frac{\partial \rho}{\partial t} + \frac{\partial(\rho U_x)}{\partial X} + \frac{\partial(\rho U_z)}{\partial Z} = 0. \quad (1)$$

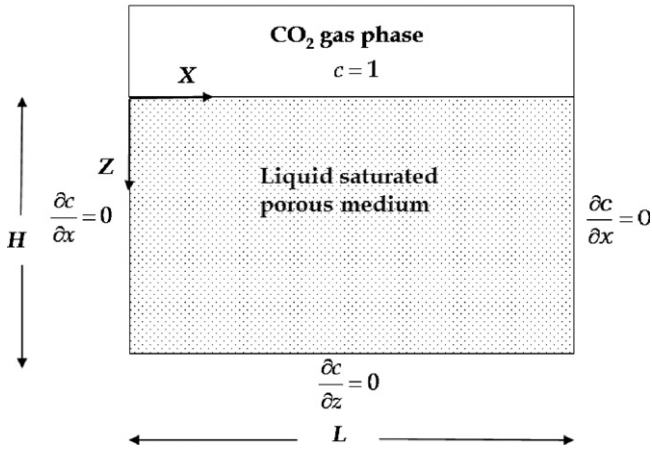


Fig. 3. Schematic of the system and coordinates.

(b) Darcy's law

$$U_x = -\frac{k}{\mu} \frac{\partial p}{\partial X}, \quad (2)$$

$$U_z = -\frac{k}{\mu} \left(\frac{\partial p}{\partial Z} - \rho g \right). \quad (3)$$

(c) Concentration

$$\frac{\phi \partial c'}{\partial t} + U_x \frac{\partial c'}{\partial X} + U_z \frac{\partial c'}{\partial Z} = \phi D \left(\frac{\partial^2 c'}{\partial X^2} + \frac{\partial^2 c'}{\partial Z^2} \right). \quad (4)$$

The fluid becomes denser when CO₂ is present at the top part of the porous medium. We assume that the liquid density changes linearly with the increasing CO₂ concentration, i.e.,

$$\rho = \rho_0(1 + \beta_c(c' - c'_0)), \quad (5)$$

from which we obtain

$$\frac{\partial \rho}{\partial X} = \rho_0 \beta \frac{\partial c'}{\partial X}. \quad (6)$$

In Eqs. (1)–(4) we have four unknowns (U_x , U_z , p and c'). It is possible to eliminate the pressure by cross-differentiating equations (2) and (3) (Eq. (2) with respect to Z and Eq. (3) with respect to X). This leads to

$$\frac{\partial U_z}{\partial X} - \frac{\partial U_x}{\partial Z} = \frac{kg\rho_0\beta}{\mu} \frac{\partial c'}{\partial X}. \quad (7)$$

Therefore, the equations to be solved are Eqs. (1), (4) and (7) to obtain U_x , U_z and c' .

3.3. Dimensionless form of the equations

We take H as characteristic length and define the following dimensionless variables

$$\begin{aligned} x &= \frac{X}{H}, \quad z = \frac{Z}{H}, \quad u_x = \frac{H}{\phi D} U_x, \quad u_z = \frac{H}{\phi D} U_z, \\ \tau &= \frac{D}{H^2} t, \quad c = \frac{c' - c'_i}{c'_0 - c'_i}, \quad u_x = -\frac{\partial \psi}{\partial z}, \quad u_z = \frac{\partial \psi}{\partial x}, \\ Ra &= \frac{k\rho_0\beta g H \Delta c'}{\phi D \mu} = \frac{\Delta \rho g k H}{\phi D \mu}. \end{aligned} \quad (8)$$

Thus, after applying the Boussinesq approximation the dimensionless form of the equations can be written as

$$\frac{\partial^2 \psi}{\partial x^2} + \frac{\partial^2 \psi}{\partial z^2} = Ra \frac{\partial c}{\partial x}, \quad (9)$$

$$\frac{\partial c}{\partial \tau} + \frac{\partial \psi}{\partial z} \frac{\partial c}{\partial x} - \frac{\partial \psi}{\partial x} \frac{\partial c}{\partial z} = \frac{\partial^2 c}{\partial x^2} + \frac{\partial^2 c}{\partial z^2}. \quad (10)$$

3.4. Boundary and initial conditions

The initial condition of the problem is

$$\psi = 0, \quad c = 0 \quad \text{at } \tau = 0. \quad (11)$$

The boundary conditions of the problem are

$$\begin{aligned} \psi &= 0, \quad \frac{\partial c}{\partial z} = 0 \quad \text{at } x = 0, \\ \psi &= 0, \quad c = 1 \quad \text{at } z = 0, \\ \psi &= 0, \quad \frac{\partial c}{\partial x} = 0 \quad \text{at } z = 1, \\ \psi &= 0, \quad \frac{\partial c}{\partial x} = 0 \quad \text{at } x = A. \end{aligned} \quad (12)$$

3.5. Solution procedure

A modified version of the numerical method explained by Guçeri and Farouk [16] was applied to solve the system of Eqs. (9) and (10), i.e., the finite volume approach. A fully implicit method was used to obtain the transient values in Eq. (10). For each time step, we first compute the stream function from Eq. (9) and then we obtain the concentration profile by solving Eq. (10). The calculation procedure for each time step was repeated until the following criteria were satisfied:

$$\left| \frac{c_{i,j}^{\tau+\Delta\tau} - c_{i,j}^{\tau}}{c_{i,j}^{\tau+\Delta\tau}} \right|_{\max} \leq \varepsilon \quad \text{and} \quad \left| \frac{\psi_{i,j}^{\tau+\Delta\tau} - \psi_{i,j}^{\tau}}{\psi_{i,j}^{\tau+\Delta\tau}} \right|_{\max} \leq \varepsilon.$$

ε was set to 10^{-5} in the numerical computations reported in this paper and the time step was chosen to be as small as 10^{-5} (for small Rayleigh numbers) and 10^{-6} (for $Ra > 1000$) to obtain accurate results. The developed code was checked with the literature benchmark [17,18] and the results were in excellent agreement with the published simulations independent of the number of grid cells.

To observe the non-linear behavior, i.e., the fingering behavior it was necessary to disturb the interface. We used sinusoidal perturbations of macroscopic wavelength. In reality fluctuations are caused by thermodynamic fluctuations (see Refs. [19,20]) and porelevel perturbations. We

ignore instabilities on the pore level (see, however, e.g., Refs. [21,22]).

4. Results and discussion

We study the stability behavior by imposing small initial perturbations. This idea is following the normal mode method which is an analytical method that investigates the stability of a system of equations to infinitesimally small perturbations. It uses the idea that any perturbation can be decomposed into its Fourier components, i.e., in our 2-D example sinusoidal perturbation. We used wavenum-

bers ($\alpha = 2\pi/\lambda$) between 10 and 270 to investigate the effect of the wavelength. The normal mode method also uses the concept of fastest growing wavelength as the characteristic wave length which will emerge as the result of an arbitrary perturbation. Following this idea it is asserted that the long term behavior does not depend on the initial perturbation and hence reflects a material or structural property. For instance we observe (see for instance Fig. 8) that after some time the number of fingers are less than the number of periods in the initial perturbation. However, Fig. 15 shows that the growth rate of the perturbations is a weak function of the wavelength. Hence there will be some tenacity of the

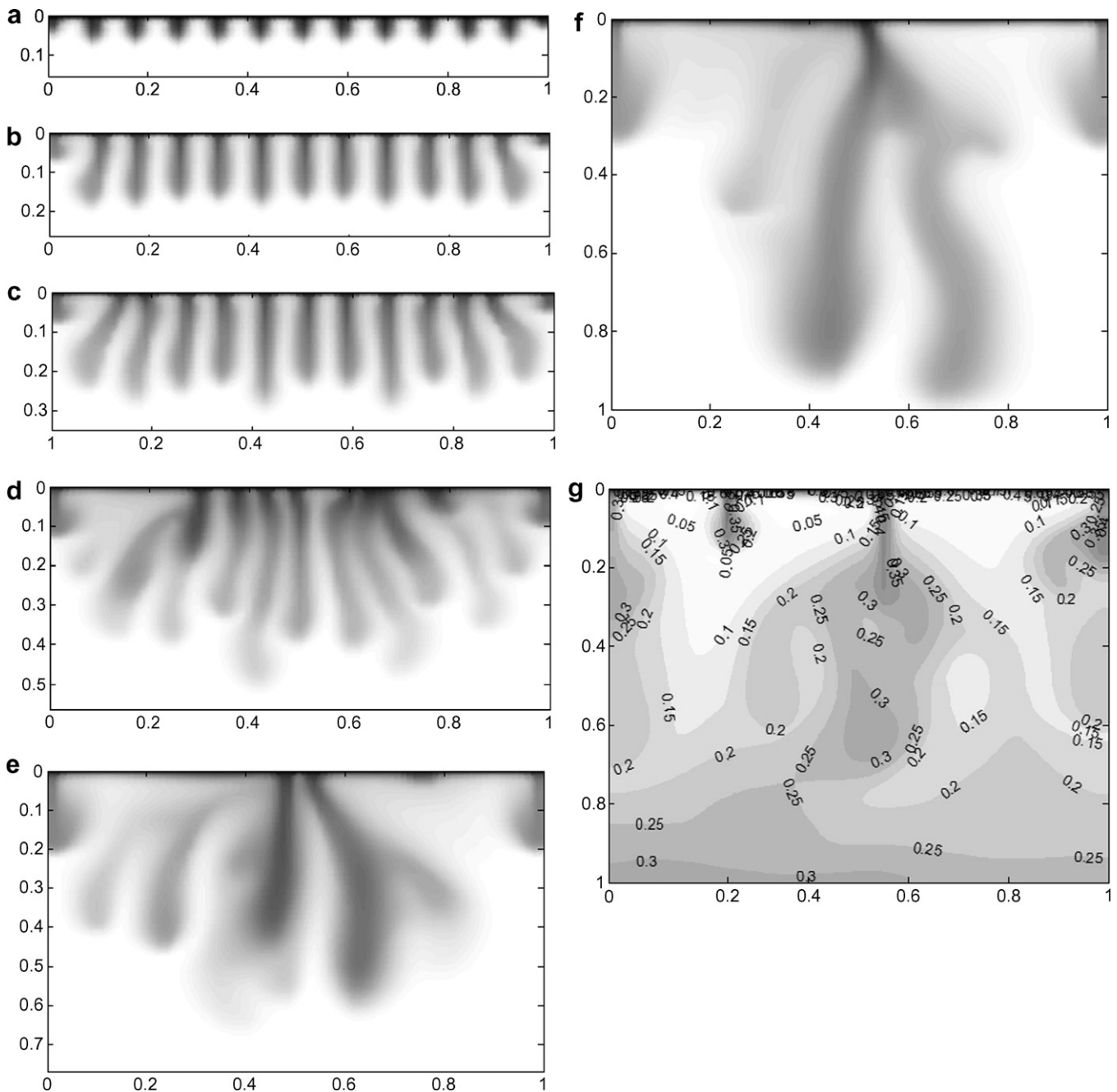


Fig. 4. Concentration profiles for $Ra = 10000$ at $\tau =$ (a) 5×10^{-5} , (b) 1.5×10^{-4} , (c) 2.5×10^{-4} , (d) 5×10^{-4} , (e) 7.5×10^{-4} , (f) 1.06×10^{-3} and (g) 0.002.

initial behavior and the pattern observed in the figures persists for some time before the number of fingers starts to decrease and starts to reflect structural properties.

It is well established that for a certain fluid the dynamics of flow in the porous medium is strongly dependent on the characteristics of the porous medium, i.e., the permeability and for the non-cubic medium the ratio of length over height (L/H). The effect of heterogeneity is neglected in this paper and we discuss the effect of the Rayleigh number (Ra) and the aspect ratio (A).

4.1. Effect of Rayleigh number

Fig. 4 shows the concentration profile for $Ra = 10000$ and $A = 1$ at different times. This simulation was performed with 81×81 grid cells. An initial perturbation, too small to be visible in the plots, was introduced in the system. Although the interface is disturbed and unstable, initially the imposed perturbation is damped and the CO_2 -rich front moves in diffusion like manner. Therefore, in the simulations some time elapses before the small fingers appear. At early times, e.g., $\tau = 5 \times 10^{-5}$ (Fig. 4a) and $\tau = 1.5 \times 10^{-4}$ (Fig. 4b), the number of fingers remain equal to the number put in the initial perturbation, i.e., 11. Nevertheless some fingers grow faster than the others (Fig. 4c). The laboratory results in the absence of a porous medium show that natural convection effects die out with time [5]. This can also be concluded from the experiment performed in a porous medium (Fig. 2). Therefore, it appears that the density difference, i.e., the driving force for natural convection decreases with time. This means that the concentration of CO_2 is distributed more evenly as more CO_2 is dissolved. In the numerical simulations this effect is also observed. In the simulations the number of fingers decreases with increasing time. It appears that the neighboring fingers coalesce by mutual interaction, a process which is governed by diffusion. This behavior has been also observed in Refs. [9–11]. A noticeable feature in our simulations is that the merging starts at the “trunk” rather than at the tip of the finger and from there it proceeds to the rest of the system. The merging of fingers continues until the end of the simulation.

Fig. 5 shows a grey level plot of the stream function for $\tau = 5 \times 10^{-4}$. Dark areas correspond to high positive values of the stream function, with a maximum value of 100. Light areas correspond to negative values, with the lowest value of -120 . Comparison with Fig. 4d shows a similarity in the contours between concentration profiles and stream function profiles. This shows the importance of natural convection for the spreading of CO_2 in the cell. Moreover, it means that the dynamics of the non-linear behavior, i.e., the fingering of the CO_2 in the porous medium is governed by the flow field. Simulation results show that at $\tau = 0.002$ the maximum and minimum values of the stream function are 80 and -90 , respectively. This indicates that the values of stream function, i.e., the velocity components, decrease with increasing time due to the

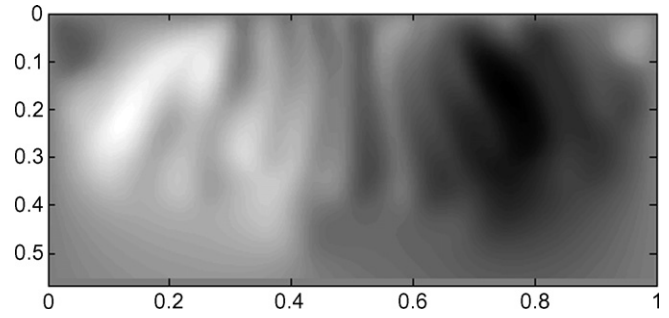


Fig. 5. Stream function profile for $Ra = 10000$ at $\tau = 5 \times 10^{-4}$ with maximum value of 100 and minimum value of -120 .

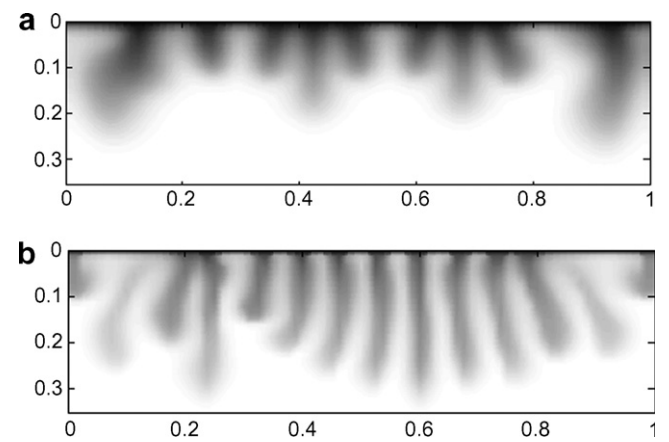


Fig. 6. Concentration profiles for (a) $Ra = 2000$ at $\tau = 1.4 \times 10^{-3}$ and (b) $Ra = 20000$ at $\tau = 1.3 \times 10^{-4}$.

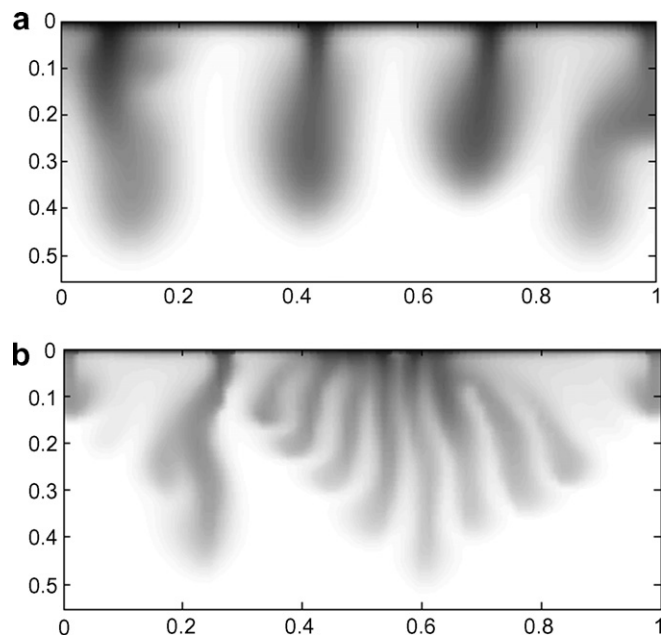


Fig. 7. Concentration profiles for $Ra = 2000$, at (a) $\tau = 2.5 \times 10^{-3}$ and (b) $Ra = 20000$ at $\tau = 2.2 \times 10^{-4}$.

increasingly more homogeneous concentration distribution as time progresses.

The concentration contours shown in Fig. 4 suggest that the late-stage behavior of the mass transfer process cannot be precisely predicted by the early-stage behavior of the

system. This complexity in the flow behavior is strongly dependent on the Rayleigh number. To show the effect of different Rayleigh numbers we plot the early-stage concentration profiles of $Ra = 2000$ and $Ra = 20000$ and compare them with the base case $Ra = 10000$. Furthermore, to show

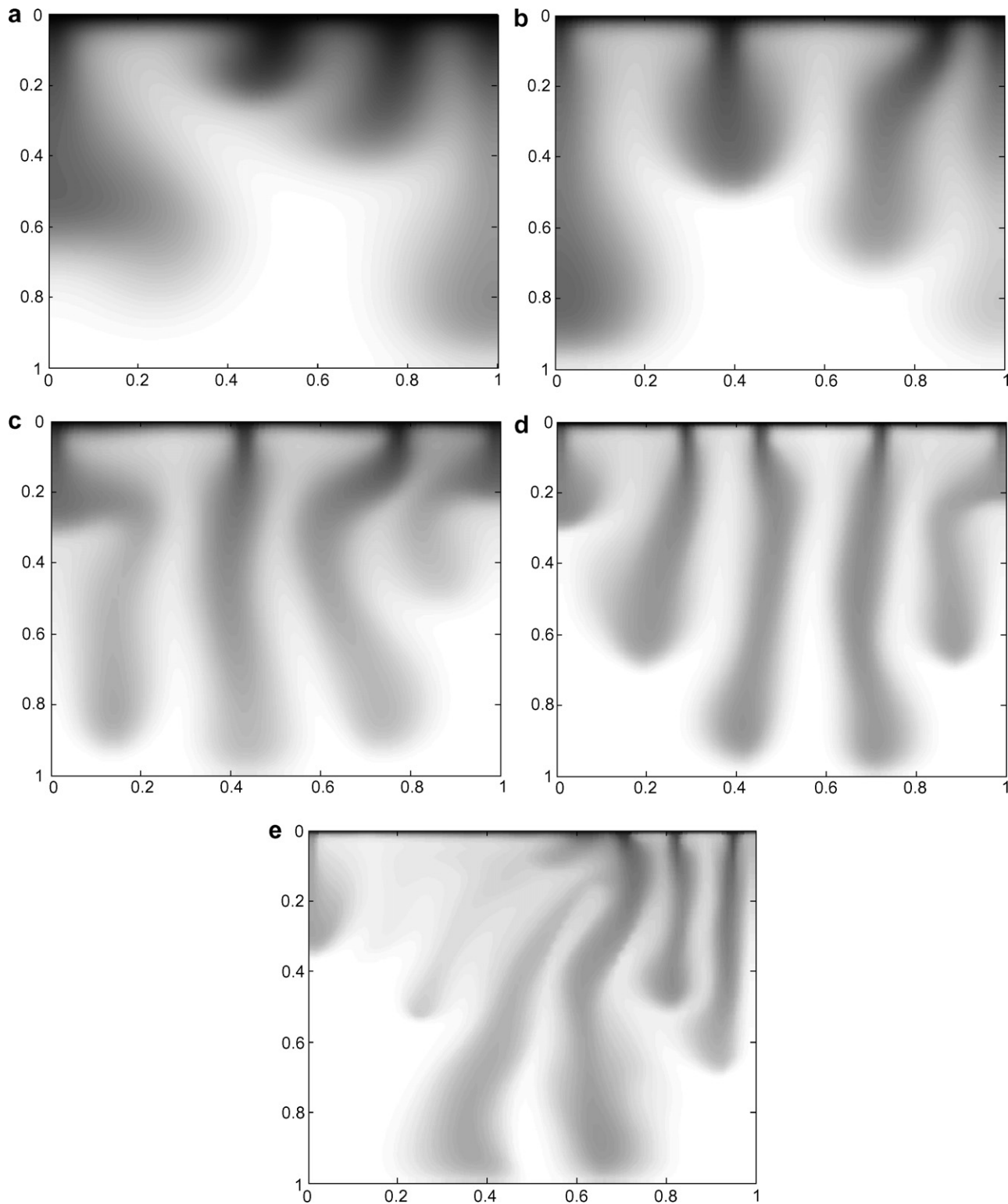


Fig. 8. Concentration profiles for (a) $Ra = 500$ at $\tau = 2.47 \times 10^{-2}$, (b) $Ra = 1000$ at $\tau = 1.06 \times 10^{-2}$, (c) $Ra = 2000$ at $\tau = 5.1 \times 10^{-3}$, (d) $Ra = 5000$ at $\tau = 2.0 \times 10^{-3}$ and (e) $Ra = 20000$ at $\tau = 6.25 \times 10^{-4}$.

the late-stage flow behavior we plot the concentration profile for $Ra = 500, 1000, 2000, 5000$ and 20000 when the CO_2 concentration of the bottom of the cell for the first time reaches 10% of the initial concentration at the top.

Fig. 6 shows the concentration contours for $Ra = 2000$ at $\tau = 1.4 \times 10^{-3}$ and $Ra = 20000$ at $\tau = 1.3 \times 10^{-4}$. Comparison of these profiles with Fig. 4c indicates that concentration front moves faster for the larger Rayleigh numbers. This means that natural convection affects the mass transfer significantly for larger Rayleigh numbers. For $Ra = 2000$ the number of fingers has been already decreased (Fig. 6a). However, some fingers merge together and form large fingers (Fig. 7a) and move without any further interactions until they reach the bottom (Fig. 8c). Comparing Figs. 6b and 7b shows that the non-linear behavior of the fingering is more pronounced at higher Rayleigh numbers. The stream function profiles corresponding to the concentration profiles shown in Fig. 7 preserve a similar pattern to the concentration profiles, as discussed previously in Fig. 5. However, the values of the stream function increase with increasing Rayleigh number.

The late-stage flow behavior of different Rayleigh numbers is shown in Fig. 8. As discussed above, for $Ra < 5000$ at the initial stages the smaller fingers merge together and progress without any significant interactions with the neighboring fingers. An interesting feature in the simulation results is that for smaller Rayleigh numbers CO_2 flows downwards close to the boundaries. In another words, the flow is faster close to the boundaries than near the center for the small Rayleigh numbers. The time in which the CO_2 front (10%) reaches the bottom of the cell is plotted in Fig. 9 for different Rayleigh numbers. This figure suggests that given the conditions of our simulations (the initial perturbation, number of grid cells, etc.) there is a linear relation between the inverse of this time and Rayleigh number. This linear relation emphasizes the importance of the convection effect compared to diffusion.

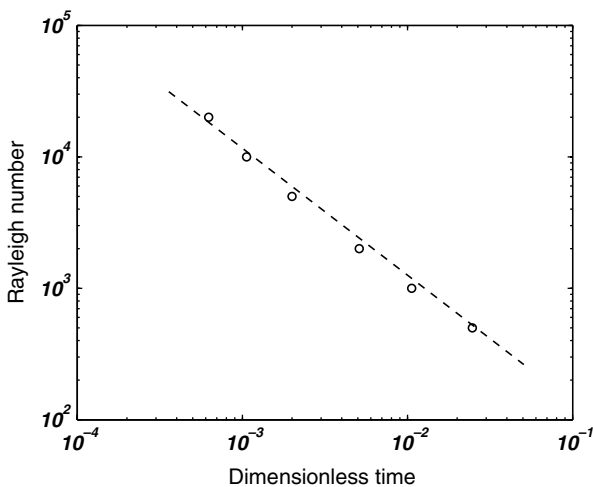


Fig. 9. The time required for the CO_2 concentration to reach to $0.1c_0$ at the bottom for the first time for different Rayleigh numbers.

Fig. 10 shows the progress of the tip position of the most advanced finger with time for different Rayleigh numbers in a log–log plot. With the term *advanced tip position* we mean the distance from the gas–liquid interface to the contour in which the CO_2 reaches 10% of the initial concentration at the top boundary. This plot shows that initially the CO_2 front moves proportional to the square-root of time, i.e., the initial behavior is controlled by diffusion. In all cases, after some time the relation becomes linear, i.e., convection starts to play a role in the system. The time, in which the relation changes to linear behavior, decreases with increasing Rayleigh number. For the number of grid cells used in our simulation it was difficult to get the exact point of the front for higher Rayleigh numbers; therefore these values are not plotted in Fig. 10.

4.2. Effect of aspect ratio

Figs. 11 and 12 show the simulation results for $Ra = 10000$ and different aspect ratios. Comparison of these plots with concentration profiles in Fig. 4 yields that the interaction between fingers decreases with increasing aspect ratio. The number of fingers that survive to reach the bottom of the cell in the $A = 4$ case is equal to the number of the initially imposed fingers indicating that the interaction between the fingers decreases with increasing the aspect ratio. Nevertheless, the time required for the 10% CO_2 front to reach the bottom increases with increasing aspect ratio.

4.3. Growth of the disturbance

In the numerical simulations presented in this paper the imposed initial disturbance was the sinusoidal disturbance with wavelength λ and amplitude δ (Fig. 13). The wave-number is defined as $\alpha = 2\pi/\lambda$. We assume that any disturbance grows exponentially

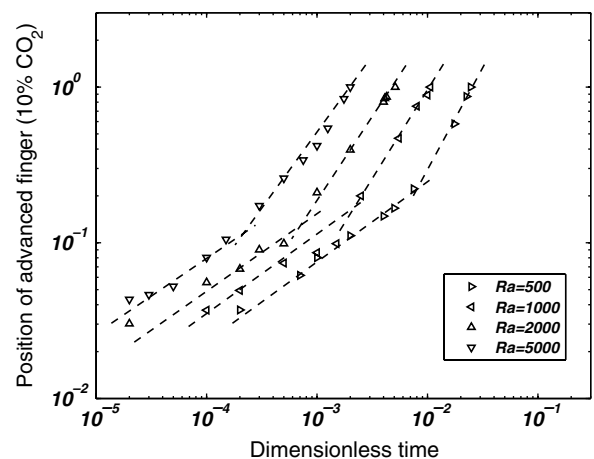


Fig. 10. Progress of the tip of the most advanced finger for different Rayleigh numbers as a function of time and the change from square-root behavior to linear behavior.

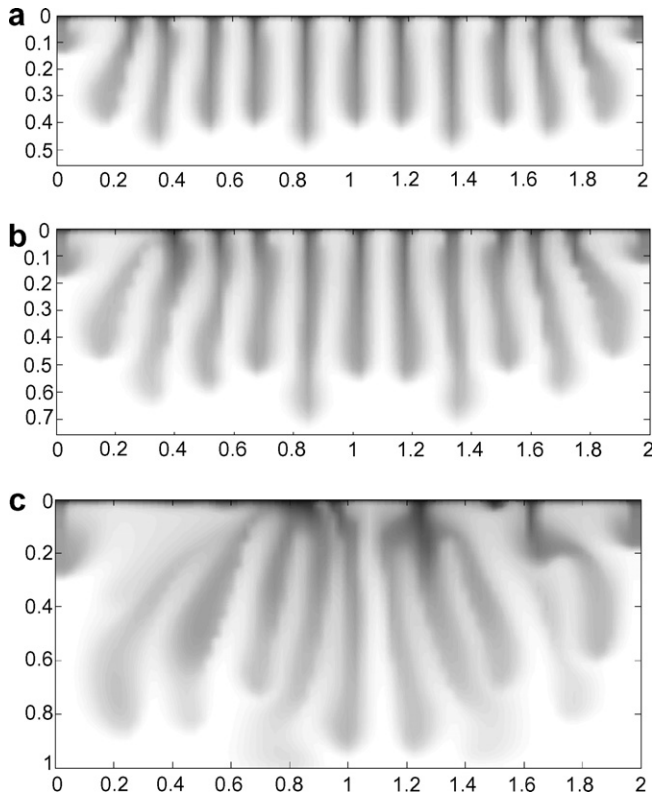


Fig. 11. Concentration profiles for $A=2$ and $Ra=10000$ at $\tau =$ (a) 5×10^{-4} , (b) 7.5×10^{-4} and (c) 1.39×10^{-3} .

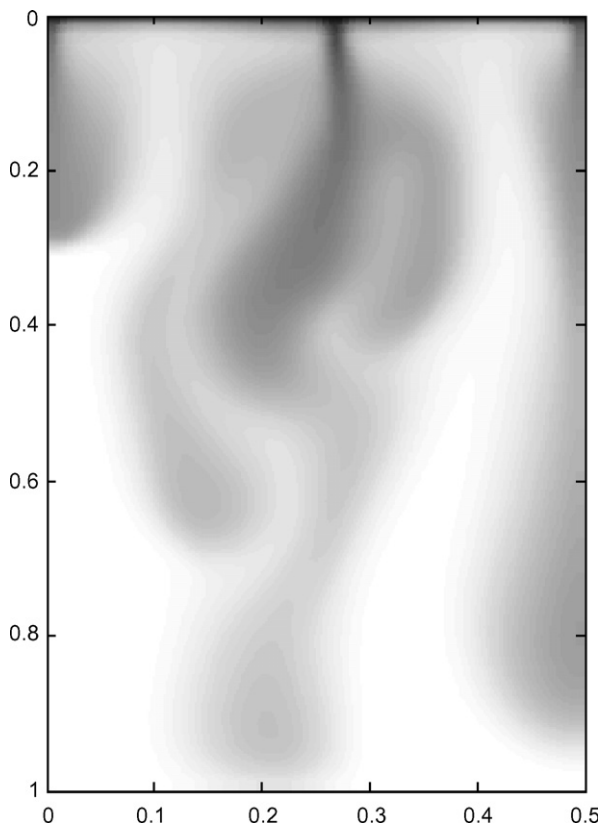


Fig. 12. Concentration profiles for $A=0.5$ and $Ra=10000$ at $\tau = 9.3 \times 10^{-4}$.

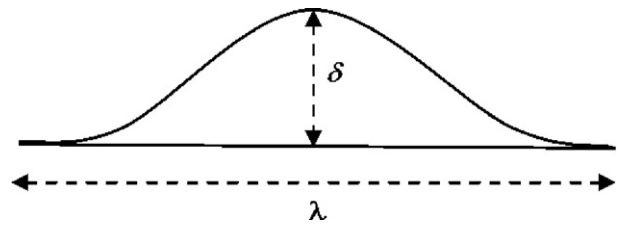


Fig. 13. Schematic of the imposed sinusoidal perturbation at the interface.

$$\delta(\tau) = \delta_0 \exp(\sigma\tau). \tag{13}$$

δ_0 is a constant, which can be determined by the initial condition of the interface, and $\sigma(\alpha)$ is the wavelength dependent disturbance growth factor. Eq. (13) means that a plot of $\ln(\delta)$ versus time is a straight line. The slope of this straight line gives the growth factor σ . Depending on the scope of σ it is possible to find the fastest growing wave-number at which the first derivative of σ towards the wave-number α becomes zero. The determination of the fastest growing wave-number is as follows.

In the simulations for a certain Rayleigh number we determine the average amplitude of one arbitrary contour line of the concentration profile (in this paper $c = 0.4$ line) for different wave-numbers. We plot the average amplitudes of the $c = 0.4$ contour line versus time in a semi-logarithmic plot. The slope of the obtained lines gives σ of the selected wave-number. We plot the obtained growth factors versus wave-number to get the value of the fastest growing wave-number.

In Fig. 14 we present plot of $\ln(\delta)$ versus time only for $Ra = 2000$ for different wave-numbers. The regression coefficient of the fitted lines were all larger than 0.97. This means that the imposed instabilities grow linearly in agreement with Eq. (13). However, it was noticed that in some simulations when we considered the late-stage points the regression coefficients became less than 0.95, suggesting that at the later stage the growth of the instabilities is not linear. Therefore, in order to find fastest growing wave-number we

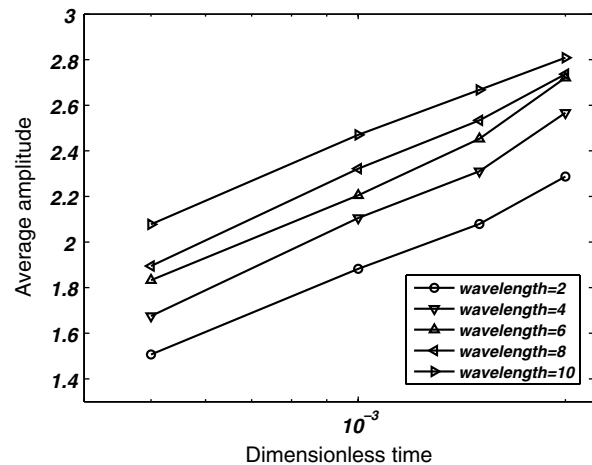


Fig. 14. Logarithm of the average amplitude (distance from interface) of the growing fingers versus time for $Ra = 2000$.

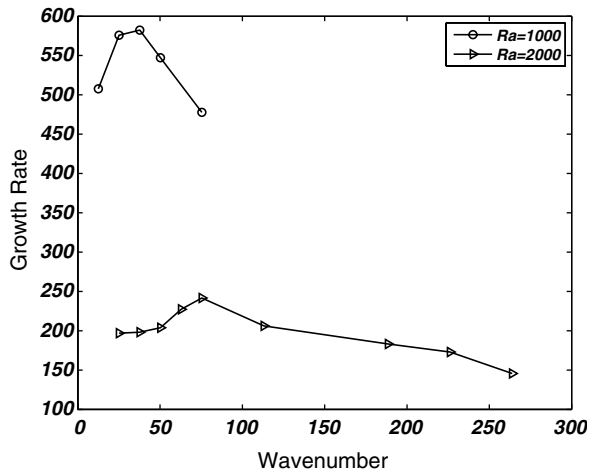


Fig. 15. Growth rate coefficient as a function of wave-number for $Ra = 1000$ and $Ra = 2000$.

Table 1
Wavelengths and corresponding growth rates for $Ra = 1000$

$1/\lambda$	σ
4	196.95
6	198.122
8	203.82
10	227.2
12	241.66
18	206.24
30	183.22
36	173.13
42	145.68

Table 2
Wavelengths and corresponding growth rates for $Ra = 2000$

$1/\lambda$	σ
2	507.68
4	575.78
6	582.32
8	547.16
10	477.72

omitted the late-stage points when the regression coefficient was less than 0.95. The non-linear growth of fingers at later stages has been also reported by Park et al. [23]. Fig. 15 shows the growth factor as a function of wave-number for $Ra = 2000$ and $Ra = 1000$. The extracted growth rates are presented in Tables 1 and 2 for $Ra = 1000$ and $Ra = 2000$, respectively. It is clear from these Tables and Fig. 15 that the fastest growing wave-number is between 50–75 for $Ra = 1000$ and 25–37 for $Ra = 2000$.

5. Conclusions

In this paper we studied the transient density-driven natural convection problem when the top of the porous medium initially saturated with a liquid is exposed to a CO_2 -

rich gaseous phase. With the aid of dimensionless groups it is possible to study the effect of different parameters on the fate of injected CO_2 into the porous medium. It is shown that the density-driven natural convection with the boundaries used in this paper has a significant effect on the mass transfer. The effect of natural convection increases with increasing Rayleigh number that depends both on the characteristics of the porous medium, mainly the permeability, and the fluid properties. With increasing aspect ratio, the time to see the beginning of the natural convection decreases. The simulation results show that the non-linear behavior of the flow is strongly dependent on the Rayleigh number. With increasing Rayleigh number natural convection effects become more significant. However, as time elapses the number of the fingers decreases due to the decreasing effect of natural convection. This effect can be also observed from the decreasing values of the stream function. Initially, the CO_2 front moves proportional to the square-root of time for different Rayleigh numbers and then the relationship becomes linear. However, the time in which the switching happens decreases with increasing Rayleigh number.

Acknowledgements

This study was supported by a special program of the TU Delft, DelftEarth Research. The authors thank the technical staff of the Dietz laboratory, especially H. v.d. Meulen for their help in conducting experiments. This paper was originally presented as SPE 107381 at the 2007 SPE EUROPEC conference, held June. 11–14 in London, UK.

References

- [1] L. Gmelin, Gmelin Handbuch der anorganischen Chemie, 8. Auflage. Kohlenstoff, Teil C3, Verbindungen, 1973, pp. 64–75.
- [2] A. Ashcroft, Isa M. Ben, Effect of dissolved gases on the densities of hydrocarbons, J. Chem. Eng. Data (1997) 1244–1248.
- [3] E. Lindeberg, D. Wessel-Berg, Vertical convection in an aquifer column under a gas cap of CO_2 , Energy Convers. Manage. 38 (1997) S229–S234.
- [4] Ch. Yang, Y. Gu, Accelerated mass transfer of CO_2 in reservoir brine due to density-driven natural convection at high pressures and elevated temperatures, Ind. Eng. Chem. Res. 45 (2006) 2430–2436.
- [5] R. Farajzadeh, A. Barati, H.A. Delil, J. Bruining, P.L.J. Zitha, Mass transfer of CO_2 into water and surfactant solutions, Pet. Sci. Technol., in press.
- [6] T.D. Foster, Stability of a homogenous fluid cooled uniformly from above, Phys. Fluids 8 (7) (1965) 1249–1257.
- [7] T.D. Foster, Onset of convection in a layer of fluid cooled from above, Phys. Fluids 8 (8) (1965) 1770–1774.
- [8] E.R. Lapwood, Convection of a fluid in a porous medium, Proc. Camb. Phil. Soc. 44 (1948) 508.
- [9] J.W. Elder, The unstable thermal interface, J. Fluid Mech. 32 (1968) 69–96.
- [10] R.A. Wooding, Growth of fingers at an unstable diffusing interface in a porous medium or Hele-Shaw cell, J. Fluid Mech. 39 (1969) 477–495.
- [11] A. Riaz, M. Hesse, A. Tchelepi, F.M. Orr, Onset of convection in a gravitationally unstable diffusive boundary layer in porous medium, J. Fluid Mech. 548 (2006) 87–111.

- [12] K.L. Walker, G.M. Homsy, Convection in a porous cavity, *J. Fluid Mech.* 87 (1978) 449–474.
- [13] J. Ennis-King, I. Preston, L. Paterson, Onset of convection in anisotropic porous media subject to a rapid change in boundary conditions, *Phys. Fluids* 17 (2005) 84107.
- [14] J.P. Caltagirone, Stability of a saturated porous layer subject to a sudden rise in surface temperature: comparison between the linear and energy methods, *J. Mech. Appl. Math.* 23 (1) (1980) 47–58.
- [15] X. Xu, Sh. Chen, D. Zhang, Convective stability analysis of the long-term storage of carbon dioxide in deep saline aquifers, *Adv. Water Res.* 29 (2006) 397–407.
- [16] S. Guçeri, B. Farouk, Numerical solutions in laminar and turbulent natural convection, in: S. Kakac, W. Aung, R. Viskanta (Eds.), *Natural Convection, Fundamentals and Applications*, Hemisphere Publication, 1985, pp. 615–655.
- [17] M. Shathiyamoorthy, T. Basak, S. Roy, I. Pop, Steady state convection flow in a square cavity filled with a porous medium for linearly heated side walls, *Int. J. Heat Mass Transfer* (2006), doi:10.1016/j.ijheatmasstransfer.2006.10.010.
- [18] A. Bahloul, Boundary layer and stability analysis of natural convection in a porous cavity, *Int. J. Therm. Sci.* 45 (2006) 635–642.
- [19] L.D. Landau, E.M. Lifshitz, *Statistical Physics: Course of Theoretical Physics*, 2nd revised English ed., vol. 5, Pergamon Press, 1969.
- [20] R.D. Gunn, W.B. Krantz, Reverse combustion instabilities in tar Sands and coal, *SPE 6735-PA* (1980).
- [21] Y.C. Yortsos, B. Xu, D. Salin, Phase diagram of fully developed drainage in porous media, *Phys. Rev. Lett.* 79 (23) (1997).
- [22] M. Parlari, Y.C. Yortsos, Percolation theory of steam/water relative permeability, *SPE 16969* (1987).
- [23] C.W. Park, S. Gorell, G.M. Homsy, Two-phase displacement in Hele-Shaw cells: experiments on viscosity driven instabilities, *J. Fluid Mech.* 141 (1984) 275–287.